Scaling Organic Electrochemical Transistors Down to Nano-sized Channels

Pasquale D'Angelo ‡, Simone L. Marasso ‡, Alessio Verna, Alberto Ballesio, Matteo Parmeggiani, Alessandro Sanginario, Giuseppe Tarabella, Danilo Demarchi, Candido F. Pirri, Matteo Cocuzza and Salvatore Iannotta*

Dr. P. D'Angelo, Dr. S. L. Marasso, Dr. M. Cocuzza, Dr. S. Iannotta.
Consiglio Nazionale delle Ricerche-Istituto dei Materiali per l'Elettronica ed il Magnetismo (IMEM), P.co Area delle Scienze 37/A, Parma, 43124, Italy
E-mail: simone.marasso@polito.it

Dr. S. L. Marasso, Dr. A. Verna, A. Ballesio, M. Parmeggiani, Prof. C. F. Pirri, Dr. M. Cocuzza
Chilab - Materials and Microsystems Laboratory, Department of Applied Science and Technology (DISAT), Politecnico di Torino, Chivasso (Turin), 10034, Italy

M. Parmeggiani, Prof. C. F. Pirri
Center for Sustainable Future Technologies, Italian Institute of Technology, Turin, 10129 Italy

Dr. A. Sanginario, Prof. D. Demarchi
Electronic and Telecommunication Department, Politecnico di Torino, 10129, Turin, 10129, Italy

Dr. G. Tarabella
Camlin Italy Srl, Strada Budellungo 2, Parma, 43123, Italy

Keywords: Nanogap-OECTs, electromigration induced break junction, electrochemical impedance spectroscopy, intercalation pseudocapacitance, organic bioelectronics.

The perspective of downscaling Organic Electrochemical Transistors (OECTs) in the nano-range is approached by depositing Poly(3,4-EthyleneDiOxyThiophene) PolyStyrene Sulfonate (PEDOT:PSS) on electrodes with a nano-gap designed and fabricated by Electromigration Induced Break Junction (EIBJ) technique. The electrical response of the fabricated devices is obtained by acquiring transfer characteristics in order to clarify the specific main characteristics of OECTs with submicrometer-sized active channels (herein referred to as Nanogap-OECTs). On the basis of their electrical response to different scan times, the Nanogap-OECT shows a maximum transconductance unaffected upon changing scan times in the time window from 1 s to 100 µs, meaning that fast varying signals can be

easily acquired with unchanged amplifying performance. Hence, the scaling down of the channel size to the nanometer scale leads to a geometrical paradigm that minimizes effects on device response due to the cationic diffusion into the polymeric channel. A comprehensive study of these features is carried out by an Electrochemical Impedance Spectroscopy (EIS) study, complemented by a quantitative analysis made by equivalent circuits. The propagation of a redox front into the polymer bulk due to ionic diffusion (also known as the 'intercalation pseudocapacitance') is identified as a limiting factor for the transduction dynamics.

1. Introduction

Organic Electrochemical Transistors (OECTs) are a family of ion sensitive devices based on the doping de-doping effect of conductive and electroactive polymers in contact with an electrolyte solution [1]. Poly(3,4-EthyleneDiOxyThiophene) PolyStyrene Sulfonate (PEDOT:PSS), a diphasic organic conductor showing a mixed ionic-electronic conduction largely used in unconventional electronics due to its peculiar features[2] [3] [4] [5], is the benchmark material for OECT manufacturing. OECTs are successfully applied to biosensing [6] [7] [8] and health monitoring [9] [10] with great advantages in terms of biocompatibility and sensitivity, at very low operating voltages (below 1V, well suited for bio-interfacing). These properties make the OECT ideal for both bio-electronics and for interfacing human body. Recent works have demonstrated real-time recording of neural signals, typically on the millisecond scale, where the detection has been achieved by both PEDOT:PSS-based electrodes [11] [12] and OECTs with micron-sized channels [13]. A fine spatio-temporal map of brain activity requires in particular OECTs combining a compact architecture and high operating speed [14]. More generally downscaling is considered an essential evolution of devices in the field of Integrated Circuit (IC) and Micro Electro Mechanical System (MEMS). The typical advantages envisaged are the compactness [15], low energy consumption [16] and large scale production [17]. The typical fees to pay are related to device heating issues [18], standard photolithography resolution limits, process compatibility, and process

optimization with respect to all the possible critical steps. Nanogap technology [19] is a top-down approach to nanopatterning, which is particularly suited to obtain electrodes with nanometric distance and hence to define a nano-sized channel for the fabrication of molecular biosensors allowing the detection of single-molecules as, for example, single nucleotides.

As far as the scaling down of the OECT channel is concerned, it represents a strategy for assembling and integrating compact devices with enhanced performance, particularly in terms of acquisition of fast varying signals. Literature offers an extensive overview on devices based on organic semiconductors with a high operating speed achieved by channel downscaling [20], such as Organic Field Effect Transistors (OFETs), whose operation is ruled by interfacial phenomena at the semiconductor/gate dielectric interface.

According to a general view, OECT operation relies on the uptake of cations through the PSS hydrophilic phase surrounding the PEDOT-rich clusters and their subsequent mutual interaction [21]. Recently, OECTs operation has been attributed to the coupling between the chemical potential of PEDOT:PSS with some Electric Double Layers (EDLs) formed at the PEDOT:PSS/electrolyte interface [22]. The plausibility of such a picture is highlighted by Electrochemical Impedance Spectroscopy (EIS) studies of the capacitive phenomena shown by PEDOT and related compounds (in the first instance, consisting of an EDL formation) that are indicated as responsible for the specific electrical and electrochemical properties of this material [23] [24]. As a matter of fact, changes in conductivity of PEDOT:PSS are basically ruled by bulk phenomena, i.e. phenomena occurring within the porosities inside the material, hence the operation of such a class of devices is intrinsically different from that of interfacial ones. The relevant difference between an OECT and an OFET covers even a wider set of aspects. In some cases, for instance, the scaling of OFETs channels below the micrometer scale can entail the arising of short-limit channel effects, mainly attributed to contact resistance issues [25] [26]. Indeed, PEDOT:PSS shows an ohmic behavior in the low field regime[27], which is a condition that is

mostly fulfilled in the case of OECTs because of their typical channel spacing and applied channel voltages, together with a very high conductivity, and both these aspects are not expected to influence the device response upon channel scaling down. The scaling down of OECTs channel is also of great interest to investigate the role of its microstructure in the device performance. This is because, due to clusters' coalescence in PEDOT:PSS films upon secondary doping by solvent annealing[28] [29], their typical size is expected to be larger than 10-20 nm (i.e. the nominal size of PEDOT grains in the as-purchased PEDOT:PSS colloidal suspension). Hence, it can be reasonably argued that a very fast in-plane, inter-cluster charge carrier transport, attributed to a quasi 1D-Variable Range Hopping for solvent annealed films [27], takes place due to the limited number of PEDOT/PSS interfaces. This implies that mobility issues at least scarcely influence the dynamic device response in the case of submicrometric channels. In this respect, even though OECTs time response deserves further studies for a more specific and exhaustive understanding, it is clear that the mechanisms at the basis of the device switching speed are different from those involved into the response of interfacial devices (i.e. OFETs). In general, it has been shown that OECT response is slower in devices with low aspect ratios (W/L<1 gives response time on the seconds scale [30]), while devices with aspect ratios around 1 show a faster operation [31] (down to 100 µs in some micrometer-sized OECT arrays [32]). Our devices show step-like I_{ds} vs. time curves upon application of a gate voltage step, (not reported here, since the study of response times will be the object of a dedicated follow-up work) but similar to those reported in a previous study [33]. Response times ranging in the millisecond scale (around 1ms) have been extracted using the procedure described elsewhere [30,33].

The present scenario suggests that OECTs with downscaled channels can absolutely conjugate compactness and fast operation speed. Nevertheless, even though OECTs technology is in a fast-evolving state, there is a lack of works investigating the effects of a nanoscale downsizing on standard, planar PEDOT:PSS-based OECT architectures. In fact, the available studies on sub-micron channel

lengths concern only vertical geometries alternative to the conventional planar ones [34] or ion gel gated devices based on different polymeric conductors [35].

In this framework, we here explore Electromigration Induced Break Junction (EIBJ) technique to produce nano-sized planar channels as an approach to improve OECTs channel downscaling. EIBJ is compatible with a top-down process [36] [37] and can be easily implemented following more traditional technological steps, thus complementing bottom-up approaches. We hence developed OECTs with nanometer-sized channels by EIBJ and investigated their electrical response to determine the main characteristics of the as-fabricated devices. We have investigated the scaling down of channel length (L) also by carrying out a comprehensive Electrochemical Impedance Spectroscopy (EIS) analysis with the aim of enlightening the role played at the nanometric scale by the uptake of ionic species in the polymer bulk and their diffusion through it that are responsible for the OECT current modulation.

2. Results and Discussion

In a traditional process, the downscaling of the OECTs channel is achieved by patterning the electrodes, hence it is limited by the resolution of the selected photolithographic process. In principle, switching from standard photolithography, performed by a traditional UltraViolet (UV) mercury lamp, to electron beam or possibly to X-ray lithography, represents an adequate solution for nanopatterning the device channel, but the needed equipment and the related processing are extremely expensive and time consuming when compared to EIBJ. In addition, EIBJ allows for a direct patterning of the gap skipping the photolithographic and etching steps. This results in reduced time and costs, while reducing processing issues. In principle, even an atomic gap can be achieved by this approach, making EIBJ a valid alternative to a bottom-up process. The major limit of this technique with respect to the e-beam lithography (EBL) or X-ray lithography is the intrinsic statistical repeatability of the process, which is correlated to the specific physical processes involved. This is the reason for which, as previously reported [38], the NanoCube system (Figure S1A) has been extensively tested to minimize such a

drawback. The final process flow (Figure 1) is the result of an intensive optimization of the design aimed at overcoming the critical process steps. Using the reported electrodes layout to define the gold (Au) micro wire, we obtained channels in the range from 100 to 250 nm, as shown by FESEM images in Figures 2A and 2B. Once the short channel is defined, the PEDOT:PSS patterning represents another critical step to face for the final device release. In this respect, different approaches have been reported in literature[39] [40]. In this work, a lift-off based on dimethylsulphoxide (DMSO) was found to be the most cost and time effective process to pattern the polymer. Delamination issues were reduced by a proper design of the PEDOT:PSS layer aligned on the channel (Figure 1D). A 2'' wafer containing the OECTs with a submicrometer long channel and a detail of the aligned PEDOT:PSS layer are reported in Figure S1B and S1C, respectively. EDS (Energy Dispersive X-ray Spectrometry) microanalysis (Figure 1E) clearly shows the atomic composition in the region of the nanogap-OECT (Table 1 and Table S2). C, S, O and S atoms refer to the polymer, while NaCl residual are also observed since the analysis was carried out after the device characterization. Si, Al, O and Au form the inorganic part of the device since they refer to Si/SiO_2 substrate and Au electrodes and related Al_2O_3 adhesion layer.

Transfer curves of the as-prepared devices provide information on their operation in terms of sensing performance and transduction efficiency of ionic to electronic signals, mainly by the evaluation of two parameters, the ON-OFF ratio and the device transconductance (g_m), respectively.

The ON-OFF ratio assesses the efficiency of an OECT in detecting ionic species interacting with its active channel. It measures the switching from the highly conductive, oxidized state of PEDOT:PSS, to the less conductive, reduced state upon an efficient Na^+ uptake through the PEDOT:PSS/NaCl aqueous solution interface.

The device transconductance, calculated as $g_m=\partial I_{ds}/\partial V_{gs}$, gives the OECT amplification of ionic signals transduced as electronic currents by the active channels. OECTs' transconductance results to be higher than for most of the ion-transducing solid-state devices[41], making them excellent amplifiers of

weak ionic signals, even at zero gate bias[42]. The transconductance curves (g_m vs. V_{gs}) show clear maxima corresponding to the typical sigmoidal-like transfer curves, examples of which are shown in Figure 3A.

As a result, transfer curves for long lasting scan rates (from t_{scan}=1 s to t_{scan}=10^{-2} s) are practically overlapping. Conversely, for I_{ds} at faster scan rates, the corresponding highest transduction efficiencies (i.e. transconductance maximum) show a relevant positive position shift (ΔV_{gs}, Figure 3B) with respect to the V_{gs} at which the peak position is located at the slowest scan rate, t_{scan}=1 s (see Figure 3C). ΔV_{gs} is hence the difference between the V_{gs} position of the transconductance peak for each transfer curve recorded at t_{scan} < 1 s and the one for the transfer curve recorded at t_{scan}=1 s. It turns out that such shift, as a function of t_{scan}, follows the nonlinear relationship: $\Delta V_{gs} \sim 1/\sqrt{t_{scan}}$. This is related to the typical conduction mechanisms in porous materials endowed with redox properties (as it is the case of PEDOT:PSS) that are often used as coatings for working electrodes of electrochemical sensors. The major advantage of a porous conducting and electroactive material is that it lowers the electrode impedance and promotes an enhancement of the charge transfer for a specific analyte because of its controlled diffusion through the material pores[43]. Red-ox reactions upon Na^+ uptake are governed by the ionic diffusion through the PEDOT:PSS pores [4] [44], hence the observed dependence of the onset voltage shift on the scan rate is consistent with the observation that device stability, reproducibility and performance upon fast varying scans can be ruled by a diffusion-limited process [45].

The device transconductance (Figure 3C) reveals a shift of its peak position (g_m^*) towards higher V_{gs} as the voltage scans become faster, while the peak height (around 1 mS) slowly varies with t_{scan}, showing a marked sublinear behavior ($g_m^* \sim (t_{scan})^{(0.009\pm0.001)}$, Figure S3). Such a slow change of g_m^* with t_{scan} means that Nanogap-OECTs can acquire fast varying signals while maintaining their performance almost unaffected, at least in the scan time window investigated here.

The ON/OFF ratio shows a reduction of at least one order of magnitude in the investigated t_{scan} window. The ON/OFF is calculated as the ratio between I_{ds} respectively at V_{gs}=-0.1 V (ON state, by convention) and V_{gs}=+0.7 V (OFF state), in this case chosen as the onset of the saturating trend of the transfer curve recorded at t_{scan}=1 s, where the absolute channel current value is indeed about 1% higher than that recorded at V_{gs}=0.8 V. The ON-OFF ratio shows a linear trend as a function of log(t_{scan}), as reported in Figure 3D. t_{scan} is an experimental parameter controlling the duration of the whole measurement and, consequently, the adaptation of the material at the applied voltage; hence, it provides information on the dynamics of processes involved in determining the device response. The drift of metal cations through the PEDOT:PSS bulk is expected to follow a relaxation-like (logarithmic) dynamics [46], hence the logarithmic trend observed in the ON-OFF ratio as a function of t_{scan} confirms the specific role that the dynamics of ionic diffusion through the polymer bulk plays on the current modulation.

The Nanogap-OECTs' response, in both sensing and amplifying operating modes, also depends on the channel biasing voltage V_{ds}. In particular, measurements performed by applying V_{ds}=-0.1 V, V_{ds}=-0.15 V and V_{ds}=-0.2 V (Figure S4A) show that the transconductance peak shifts towards lower V_{gs} for increasing V_{ds}, while its magnitude g_m^* and the device ON-OFF ratio (Figure S4B) both increase linearly with the channel voltage for low V_{ds} [33]. We therefore have a clear evidence that the device amplification does not depend on the scan rate in the investigated t_{scan} range, while the modulation is conversely significantly affected by the duration of the measurement. Hence, Nanogap-OECTs respond quite efficiently to fast varying signals while, on the other hand, the current modulation (i.e. the figure of merit of OECTs operating in sensor mode) provides a better sensitivity under longer lasting measurements. This result represents another strong indication that the device operation is controlled by diffusion mechanisms involving the cationic (de)dopant agents. On this basis, the device electrical response evidences the need of specific measurements assessing the PEDOT:PSS films capacitance

upon cationic diffusion. Actually, in the discussion on the origin of capacitive effects in PEDOT:PSS, different specific mechanisms have been invoked including, for instance, the formation of an EDL at the interface between PEDOT grains and PSS shells[24], where ionic diffusion, which is mainly mediated by PSS hydrophilicity[47], plays a key role. Actually, PEDOT:PSS behaves as an ideal volumetric electrochemical capacitor, with high volumetric capacitance, giving rise to the high gain in ion-to-electron transduction by OECTs[48]. An additional capacitive-like contribution is attributed to a charge transfer mechanism at the diffusing PEDOT:PSS/electrolyte interface, also known as the intercalation pseudocapacitance [49]. Intercalation pseudocapacitance influences the device response in terms of its kinetics. In fact, even if EIS demonstrates the presence of an EDL capacitance (in the context of an operation generally attributed to red-ox mechanisms), the diffusion of the electrolyte interface into the polymer bulk can induce faradaic reactions (i.e. conductivity changes) at this "pseudocapacitive" interface that may spatially evolve and cover wider fractions of the polymer bulk during the measurement. Furthermore, V_{gs} assists the propagation of this ionic front. For these reasons, depending on the device size scale, the demonstrated facile ionic diffusion into the polymer bulk [42] can evolve on the timescales of the performed measurements, as indicated by dedicated moving front experiments [50]. Hence, Nanogap-OECTs embody a prototypical geometry suitable for enlightening, via EIS, the interaction between diffusing cations and PEDOT clusters. For comparison, we also carried out EIS on a stripe-like OECT. This configuration represents, in fact, a typical PEDOT:PSS/electrolyte interface spatially variable during the measurements, while in Nanogap-OECTs such evolution is expected to saturate on a short time scale because of the combined effect of the compact device geometry and the active channel properties (i.e. channel size, electrolyte positioning and PEDOT:PSS ion mobility). In addition, even if EIS onto OECTs describes the point of view of the gate circuit, thus excluding the effect of V_{ds} on the dynamics of cationic diffusion, the role of the device channel length discussed in

some papers [51] [52] can be minimized by the nanometric longitudinal extent of Nanogap-OECTs channels.

EIS measurements consist in acquiring the Bode plots, showing both the modulus of the impedance (Z) and the phase angle as a function of the logarithm of the applied frequency (ω). On the other hand, the Nyquist plot gives the representation of the impedance in the complex plane (Z=Z'+iZ''), i.e. Z'' as a function of the real part of the impedance Z', which are related to the capacitive and resistive contributions of the thin polymeric film, respectively. This is done by short-circuiting the source and drain electrodes so that, in the limit of the short channel approximation fulfilled by our Nanogap-OECTs, such devices can be considered as a conventional coated electrode, where the PEDOT:PSS film covering the Au acts as the working electrode. The role of a negative dc bias applied to the PEDOT:PSS-covered Au electrode favors the cationic uptake by the polymer, as it happens when a positive voltage is applied to a standard Ag/AgCl electrode used as gate electrode in an OECT in a NaCl (0.1 M, in our case) aqueous electrolytic solution (gate electrolyte). In fact, for metal/electrolyte systems showing a faradaic behavior, a very small voltage drop at the gate electrode/electrolyte interfaces is expected [53]. Hence, the dc bias simulates the effective voltage applied to an Ag/AgCl electrode used as gate and immersed in a NaCl aqueous solution.

Bode plots (reported in Figure S5) provide an interesting basis for insight. The phase angle vs. log ω plot (Figure S5A) indicates that stripe-like OECTs show a dominating contribution of capacitive effects (theoretical phase angle of 90°) at low frequencies, where an important contribution of diffusion (theoretical phase angle of 45°) emerges upon gate biasing, which is likely an indication of the evolution of the intercalation pseudocapacitance. The middle-frequency region (approximately from 1 to 10 kHz in both cases) is characterized by a dominating resistive character (theoretical phase angle of 0°) followed by a reemerging capacitive contribution at higher frequencies. Taking into account the features of the applied ac signal and the typical ionic mobility in PEDOT:PSS[50], at 1 kHz the mean

displacement of an ion intercalated via the PSS phase occurs on a length scale comparable to the typical spacing between adjacent PEDOT clusters (typically, ≤1 nm [27]). All the above contributions may be therefore ascribed to the intrinsic features of the PEDOT:PSS microstructure. On the other hand, the frequency response for Nanogap-OECT (Figure S5B) shows that contributions due to diffusion are mostly probed by the spectroscopic analysis of impedance, especially at low and high frequencies.

From the log Z vs. log ω plots (Figures S5C and S5D), we extracted an equivalent capacitance C_{eq} for the geometries under study (calculated as $C_{eq}=1/(2\pi\omega Z'')$). Such an effective capacitance, accounts for all the capacitive contributions to the total capacitance (i.e. independently from their nature). Nanogap-OECTs (Figure 4A) show a more stable equivalent capacitance upon cationic injection driven by the negative dc bias, with a higher magnitude at low frequencies (dc limit). This is an effect ascribable to the device geometry while the much more pronounced drop of C_{eq} shown by stripe-like OECTs (Figure 4B), taking place even at low dc biases, likely indicates the electrolyte/PEDOT:PSS interface evolution due to the already mentioned diffusion mechanisms, i.e. the invoked intercalation pseudocapacitance [49]. This is quite different than the mentioned trends in OECTs with a submicrometric short-channel and a spatially confined PEDOT:PSS channel where, indeed, the pseudocapacitive effect due to intercalation is expected to faster saturate. The pseudocapacitive contribution associated to the cationic intercalation for stripe-like OECTs, indeed translates into the well-known initial instability (that has historically led to the introduction of the modulation parameter) shown by upscaled devices having an electrolyte interface only partially covering the channel [30] [47].

Nyquist plots in presence of negative dc biases (Figures 4C and 4D) show in both cases semicircles at high frequencies. A semicircle in the Nyquist plot for coated electrodes represents the fingerprint of charge transfer mechanisms [54] assisted by the conducting and ion permeable coverage at the working electrode [55]. The presence of a significant pseudocapacitance can be evinced from the arising of semicircles at high frequencies in the Nyquist plot; this is because the pseudo-capacitance is related to

charge transfer mechanisms [23]. The semicircles and their extent are more pronounced in the case of stripe-like OECTs, with an enlargement of their radius at increasing applied dc voltages. This is an indication of redox reactions occurring over wider fractions of the PEDOT:PSS channel bulk that certify the effective contribution of intercalation pseudocapacitance for this geometry. Such semicircles are rather depressed, if observable at all, in the case of Nanogap-OECTs, indicating a limited effect of charge transfer mechanisms ascribable to the intercalation pseudocapacitance. Indeed, the behavior at low frequencies (corresponding to the region of high Z' values) may be originated by capacitive effects or by the contribution of the ionic diffusion (mass transport). It is worth noting that control experiments have shown high reproducibility of EIS measurements. Standard deviations calculated upon repeated measurements on selected samples are four orders of magnitude lower than the corresponding impedance values.

The above results confirm that the effect of the ionic diffusion is assisted by the dc voltage biasing in both cases and, as expected, a more pronounced effect of ionic diffusion into the PEDOT:PSS bulk is found in the case of stripe-like OECTs. However, the contribution of the ionic diffusion for Nanogap-OECTs is evident also at lower dc biases, as the compact geometry of the device allows discriminating an efficient spontaneous diffusion due to the concentration gradient at the PEDOT:PSS/electrolyte interface.

Our results corroborate what it has been extensively demonstrated and rationalized about polymer-coated electrodes, where the presence of a crossover between a high frequency regime, dominated by a charge transfer between the electrolyte and the PEDOT:PSS coating (semicircles in Nyquist plots), and a low frequency regime, controlled by diffusion mechanisms (straight lines in Nyquist plots), takes place. In the case of Nanogap-OECTs, such crossover takes place at higher frequencies, showing that the contribution of diffusion mechanisms to the film dedoping is already activated on time scales of tens of microseconds (i.e. crossover frequencies ranging between 1 and 10 kHz), which are one-two orders

of magnitude shorter than those observed in stripe-like OECTs. Hence, the faster observed response to a given gate electrode voltage is the combined result of diffusion mechanisms and device geometry. In particular, our results show that pseudocapacitive effects scarcely influence the response time in Nanogap-OECTs. This observation is also coherent with the fact that very short channels reduce the inter-cluster hopping [56] that limits the device operating speed.

The resistive contribution to the overall impedance in correspondence of the above-mentioned crossover (R_{cross}) can be extracted from the Z' at the inflection points of Nyquist plots. This contribution, (plotted as a function of $V_{dc\ bias}$ in Figures 5A and 5B for Nanogap and stripe-like OECTs, respectively, shows an exponential decay. The decay can be described as $\Delta R_{cross} \sim R_0 \exp(-V_{dc\ bias}/V_{dc\ bias,activ})$, where R_0 and $V_{dc\ bias,activ}$ represent the intrinsic resistance of the device at the crossover frequency and the voltage at which the cationic drift activates the PEDOT:PSS conductivity switch, respectively. We extracted $V_{dc\ bias,activ}$ via a fitting procedure obtaining a value of about 0.14 V in both cases, indicating that the device geometry, which is known to mainly influence the gain [41], is not playing a major role on the onset voltage. Hence, $V_{dc\ bias,activ}$ depends mostly on the material's (gate and channel) properties. R_0 turns out to be 292 Ω and 2702 Ω for Nanogap and stripe-like OECTs, respectively, well compatible with the static resistances of 300 Ω and 4000 Ω assessed from I-V tests (that result to be slightly higher). In particular, the difference between the resistance assessed by EIS and the I-V analysis has been found to be larger for the stripe-like configuration. Such an occurrence well reflects the role played by diffusion mechanisms in stripe-like channels on timescales comparable to those typical for electrical measurements. This is further confirmed by the capacitive behavior at the crossover. The calculated equivalent capacitances as a function of the applied $V_{dc\ bias}$ show that capacitance is rather affected by the device geometry. In fact, we observed different behaviors of C_{eq} that, for stripe-like OECTs, consist of a monotonic linear decay (slope $7.2*10^{-6}$, Figure 5C) ascribable to the drift induced by the dc bias along the channel, while for a Nanogap-OECT, we found a marked increase of C_{eq} at $V_{dc\ bias}$= -0.4 V,

followed by a linear decrease that appears similar but with a lower slope ($1.3*10^{-7}$) with respect to that shown by the devices with a long channel (Figure 5D, dashed line as a guide to the eye).

EIS quantitative analysis is based, indeed, on equivalent circuit representations. However, the phenomenological character of this approach does not give a direct association between a true phenomenon (namely, a description derived from accurate physical-chemical models) and the circuit elements. The equivalent circuit must hence be rationalized from mechanisms which are reasonably at the basis of the phenomenon under study. We then referred to studies of electrodes coated by conducting polymers, describing the electrochemical response by means of a Mixed Kinetic-Charge Transfer Control equivalent circuit taking into account the ionic diffusion through the film pores[57] [58]. In our case, the circuit consists of a Randles Mixed Kinetic-Charge Transfer Control equivalent circuit in series with a third element (Figure 6A), namely: (i) a resistive element describing the ionic conductivity of the electrolyte; (ii) a Constant Phase Element containing info on the intercalation pseudocapacitance (QPE_{pseudo}) in parallel to a series made of a charge transfer resistance (R_{ch-tr}) and the Warburg impedance (W) that takes into account the diffusive contribution to the impedance; (iii) a parallel between C_{EDL} (describing the 'intrinsic' electrical double layer capacitance formation) and a resistor (R_{intr}) due to the intrinsic charge carrier transport. (i) and (ii) realize the Mixed Kinetic-Charge Transfer Control equivalent circuit while the latter element considers that Nanogap-OECTs show a second, much larger semicircle, in the low frequency regions of the Nyquist plots (see Figure 4C, black symbols/line curve). It is worth noting that, due to the finite thickness of the coverage, capacitive phenomena are described by constant phase elements (CPE), rather than by an ideal capacitance (ideal case of semi-infinite diffusion through film pores). CPE are described by an admittance $Y=1/Z=Q_0(j\omega)^n$, where the ideality factor n satisfies the condition $0<n<1$ and $n=1$ implies $Y=1/Z=C(j\omega)$, which is the admittance of a capacitor.

The evaluation of equivalent circuit elements, reported in Figures 6 (B-H), has been carried out through a fitting procedure (fitting curves are reported in Figures 4C and 4D). From this approach the following are the characteristics of the elements for the Nanogap-OECT:

(i) the resistive contribution coming from the ionic conduction through the electrolyte, exponentially decreases as a function of negative $V_{dc\ bias}$ ($R_{el} = 53[\Omega] - 7[\Omega]\exp(-V_{dc\ bias}/0.45[V])$, Figure 6B);

(ii) $R_{ch\text{-}tr}$ exponentially increases with negative $V_{dc\ bias}$, indicating that the extent of PEDOT:PSS bulk actually dedoped depends on the driving force regulating the cationic uptake, with an activation bias of -0.15V ($R_{ch\text{-}tr} = 230[\Omega] + 2.6[\Omega]\ \exp(-V_{dc\ bias}/0.15[V])$, Figure 6C);

(iii) QPE_{pseudo} enhances upon cationic uptake ($QPE_{pseudo} = 0.016[S\text{-}s^n] + 5.6*10^{-3}[S\text{-}s^n](\exp\text{-}V_{dc\ bias}/0.15[V])$, Figure 6D), since the electric field-assisted intercalation of cations clearly establishes a wider capacitive interface for $V_{dc\ bias} < -0.15V$. The activation bias is equal to that of $R_{ch\text{-}tr}$, meaning that our hypothesis about the role of intercalation pseudocapacitance as promoter of time-evolving charge transfer mechanisms is consistent with (and confirmed by) experimental data. In addition, by analogy with what it has been observed for R_{cross}, where a similar value of -0.14V has been found for the activation bias, such low value of -0.15V further indicates that voltage-activated pseudocapacitive processes are an intrinsic property of the material (and its microstructure);

(iv) the decrease of the ideality factor, n, upon $V_{dc\ bias}$ application mirrors the non-ideality of pseudocapacitive elements; n shows an ever increasing trend, stronger for $V_{dc\ bias} < -0.4V$ ($n = 1 + 0.48*V_{dc\ bias}$ for $V_{dc\ bias}<-0.4$ V and $n = 0.93 + 0.014*V_{dc\ bias}$ for $V_{dc\ bias}>-0.4$ V; Figure 6E);

(v) the Warburg coefficient, W, is almost unchanged up to $V_{dc\ bias} = -0.6$ V (Figure 6F), showing a drastic increase at -0.8 V that, on its turn, implies that the injection of cations at this biasing voltage does not contribute significantly to the dedoping process. This is clearly shown by the region where I_{ds} vs. V_{gs} curves show an almost saturating trend (Figure 3A);

(vi) the as-built EDL enhances as QPE_{pseudo} (C_{EDL} = 1.2[µF] + 0.7*10^{-4}[µF]exp(-$V_{dc\ bias}$/0.01[V]), Figure 6G), but its enhancement is strongly assisted by the dc bias also at very low values ($V_{dc\ bias,active}$ = -0.01V). This is indicative of the largely documented intrinsic attitude of PEDOT:PSS at facilitating capacitive phenomena;

(vii) the increase of the resistive element simulating the intrinsic charge transport (R_{intr}= 3.2*10^{3}[Ω] + 30[Ω]exp(-$V_{dc\ bias}$/0.2[V]), Figure 6H) is a further indication of the easy dedoping of PEDOT:PSS assisted by $V_{dc\ bias}$.

Fitting parameters extracted for a stripe-like OECT are reported in Table 2. Here, a Mixed Kinetic-Charge Transfer Control equivalent circuit in series with a constant phase element, named QPE2, has been used to fit the Nyquist plots in Figure 4D. QPE2 has been introduced to take into account the expected high intercalation pseudocapacitance. First of all, the experimental results show that the contribution of QPE1 of the Mixed Kinetic-Charge Transfer Control equivalent circuit is constant and denotes a purely capacitive nature, as the ideality factor is about 1 in all cases. QPE2 instead shows a peak value at $V_{dc\ bias}$=-0.4 V and is active for dc bias voltages determining an appreciable current modulation. In fact, as shown in Figures 7A and 7B, at $V_{dc\ bias}$=-0.8 V the current modulation is no more effective (saturating trend above V_{gs}= 0.6V) and the experimental data are well fitted by the Mixed Kinetic-Charge Transfer Control equivalent circuit alone.

$R_{ch\text{-}tr}$ is clearly higher than that found for the Nanogap-OECTs and drops down by one order of magnitude in the range of applied dc voltages ($R_{ch\text{-}tr}$ = R_0exp[-$V_{dc\ bias}$/0.14] + R_0^*, where R_0=37 Ω and R_0^*=1565 Ω, Figure 7C). This behavior reminds again of the materials intrinsic features, being $V_{dc\ bias,active}$ = -0.14 V as observed in the case of Nanogap-OECT. $R_{ch\text{-}tr}$ reduction is less pronounced for Nanogap-OECTs (here, the reduction is limited to a factor 5).

As far as W is concerned, unlike for Nanogap-OECTs, it decays exponentially over the whole investigated range of dc voltage biases as: W = W_0exp[-$V_{dc\ bias}$/0.14] + W_0^*, where W_0=160 Ω*s$^{-½}$ and

W_0^*=1250 Ω*$s^{-½}$ (Figure 7D). Based on the size of a stripe-like OECT channel, one would expect the diffusion driven by the electric field to be finely and easily appreciable in the case of long channels, as shown by the high and largely varying Warburg coefficients. The final remark is that the drift of cations changes their spatial distribution in the polymer bulk, and hence the pseudocapacitive interface, over timescales compatible with the lower crossover frequencies shown by stripe-like OECTs (Figure 4D). Hence, as confirmed by the observed W vs. $V_{dc\ bias}$ trend, one may conclude that the response time in this case is limited by variations of the effective cationic drift on the investigated time scale, rather than by the intrinsic conduction properties of PEDOT:PSS.

3. Conclusion

Our thorough study of OECTs with submicrometric channel sizes, fabricated on electrode gaps obtained by the EIBJ, further clarifies the mechanisms underlying the performance of such devices and the key parameters determining their characteristics. We confirm the expectation that an OECT, when properly downscaled in size, shows both superior amplifying properties of fast varying signals that remain almost unvaried in the scan time window considered in this study (from 1 s down to 100 μs) and fast response, at least on the millisecond scale. We give a clear evidence that such devices allow minimizing the role of ion diffusion on their operation, as demonstrated by the saturation of the contribution of intercalation pseudocapacitance to the device response, taking place over timescales below hundreds of microseconds. The careful EIS data analysis, supported by the use of a Randles Mixed Kinetic-Charge Transfer Control equivalent circuit and by comparison with devices with larger channel lengths, has shown that the role of intercalation pseudocapacitance in promoting charge transfer mechanisms evolving during the measurement is actually confirmed by experimental data. In addition, red-ox front propagation due to ionic diffusion assisted by V_{gs} (modeled by using a Warburg element) is responsible for the PEDOT:PSS conductivity change as long as there is some polymer bulk available for ions to move towards. Hence, downscaled electrode channels and PEDOT:PSS film sizes play a key

role in enhancing the device operation speed. From our results, it emerges that the parameters and architectures of optimized nano-scaled OECTs could be further developed, since we were able to distinguish the different contributions due to the different capacitances and resistances and, above all, their role in the final device performance. In addition, Nanogap-OECTs response time requires a detailed follow-up study (currently under way) because nanogap technology is eligible for OECTs interfacing with the human body for a proper and specific bio-signal analysis, being all of it implemented by means of compact structures that are well suited for microelectronic circuits and compact device arrays manufacturing.

4. Experimental Section

Materials. AZ 1518 and AZ 5214E photoresists have been purchased from Microchemicals-GmbH; PEDOT:PSS aqueous suspension (Clevios PH1000) has been purchased from Heraeus Holding-GmbH; ethylene glycol (EG), dodecylbenzenesulphonic acid (DBSA), dimethylsulphoxide (DMSO), isopropyl alcohol (IPA) and NaCl 1M aqueous solution have been purchased from Sigma Aldrich; Ag/AgCl electrodes have been purchased from Warner Instruments.

OECT fabrication. Nanogap-OECTs have been fabricated starting from standard 2'' wafers finished with 1 µm thermal oxide. A circular layout array of 10 OECTs with Au electrodes (Figure S1B) was designed to optimize the PEDOT:PSS deposition by spin coating. A specific layout of the Au micro wire (Figure 1A inset) (8 µm in length and 2 µm in width) was used to obtain the EIBJ, which constitutes the nanometric gap between source and drain electrodes and, hence, defines the channel length of the Nanogap-OECT.

An e-beam evaporator (ULVAC EBX-14D) was employed for the Al_2O_3/Au (thickness 20 nm / 100 nm) bilayer deposition for the source and drain electrodes. Traditional adhesion layer metals, such as Ti or Cr, should be avoided since they negatively affect the EIBJ [59] shunting the controlled electromigration in the main electrical path along the narrow Au micro wire, while Al_2O_3 acts both as a

proper adhesion layer and insulator for the EIBJ process. The use of Al_2O_3 ensures an optimal adhesion, which is peculiar for this application, as for other specific applications [60], since the induced electromigration can result in a delamination of the whole Au film. The Au patterning was performed by photolithography (with AZ 1518 photoresist) and wet etch processes employing a KI/I_2 solution (KI: I_2: H_2O = 4 g: 1 g: 40 ml). EIBJ was implemented by the NanoCube system in a customized 3D printed contacting platform (Figure S1A). This latter allows switching between the devices without damaging the contacting pads[38]. The feedback algorithm of NanoCube allows implementing the EIBJ by imposing a proper current to the Au micro wire, through a closed loop control. After that, a PECVD SiO_2 passivation layer (150 nm thick) was deposited and properly patterned. To open the windows through the SiO_2 layer in correspondence of the nanometric gaps, a photolithographic step was performed using AZ 5214E photoresist. Then, after an O_2 plasma activation of the surface, the PEDOT:PSS mixed with EG (20:1 in volume) and DBSA (0.05%,) was spin-coated on the wafer twice, to obtain a 260 nm-thick film. The PEDOT:PSS was then annealed at 150°C in vacuum for 90 min and patterned by lift-off in DMSO at 60 °C for 1 h with a final rinse in IPA.

130 nm thick stripe-like OECTs with channel length L=2 cm and an aspect ratio (W/L) =0.05 have been fabricated following the same protocol. Electrolyte has been confined at the center of the stripe by a round shaped PDMS well (∅ 5 mm).

FESEM and optical microscopy analysis. The as-fabricated channels have been characterized by ZEISS Merlin Field Emission Scanning Electron Microscopy (EHT of 5 KV). EDS microanalyses were carried out using a Zeiss Supra 40 equipped with an Oxford Liquid-N2 cooled Si(Li) detector and the Inca software for the plots and table data.

The optical micrograph of the PEDOT:PSS layer aligned with the channel region has been performed by optical microscopy (Nikon Eclipse ME600).

Nanogap-OECT electrical characterization. The electrical characterization of Nanogap-OECTs consists of recording the device response under specific measurement conditions aimed at enlightening how efficiently the device can respond to fast varying input signals. To this end, the channel current (I_{ds}) variation upon gate voltage (V_{gs}) scan sweep, in presence of 0.1 M NaCl aqueous solution with an Ag/AgCl electrode immersed in (gate electrode), has been recorded by varying V_{gs} between -0.1 V and 0.8 V (gate voltage scan step of 0.01 V) for a fixed channel voltage (V_{ds}) value of -0.2 V, using a 2-channel source-meter precision unit (Agilent B2902A). The V_{gs} scan rate (t_{scan}) has been systematically varied by one order of magnitude (from 100 µs to 1 s) from one measurement to the next.

Nanogap-OECT electrochemical characterization. By using an Ag/AgCl reference electrode and a platinum wire as counter electrode, and by applying an AC signal of ± 10 mV peak with a superimposed negative dc contribution ($V_{dc\ bias}$, varying from 0 to -0.8 V, step -0.2 V), Bode and Nyquist plots have been recorded in the frequency range 100 Hz-1 MHz using a Palmsens4 potentiostat/impedance analyzer. All the measurements have been carried out using NaCl solutions (the intention is to magnify the drift of electroactive ionic species upon application of the dc bias).

A comparison between the EIS data of Nanogap-OECTs with those obtained for a stripe-like OECT recorded in the frequency range 1 Hz-1 MHz, is provided.

Supporting Information

Supporting Information is available from the Wiley Online Library or from the author. Nanogap-OECT fabrication: Nanocube system; optical image of the PEDOT:PSS after lift-off process; devices fabricated on 2'' wafer (S1); EDS characterization in an area out of the channel (S2). Dependence of Nanogap-OECT transconductance peak positions as a function of the scan rate used for transfer characteristics measurements (S3). Dependence of Nanogap-OECT transconductance peak position and of ON-OFF ratio on channel voltage biasing. (S4). Bode plots acquired for stripe-like OECT and Nanogap-OECT in presence of a dc bias superimposed to the ac-probing signal (S5).

Acknowledgements

S.I., P.D.A., S.L.M., M.C. and G.T. gratefully acknowledge the financial support of the CARIPARMA foundation.

‡These authors contributed equally. All authors have given approval to the final version of the manuscript.

Received: ((will be filled in by the editorial staff))
Revised: ((will be filled in by the editorial staff))
Published online: ((will be filled in by the editorial staff))

References

[1] J. Rivnay, S. Inal, A. Salleo, R. M. Owens, M. Berggren, G. G. Malliaras, *Nat. Rev. Mater.* **2018**, *3*, 17086.

[2] H.-S. Park, S.-J. Ko, J.-S. Park, J. Y. Kim, H.-K. Song, *Sci. Rep.* **2013**, *3*, 2454.

[3] K. Reuter, S. Kirchmeyer, A. Elschner, in *Handb. Thiophene-Based Mater.*, John Wiley & Sons, Ltd, Chichester, UK, **2009**, pp. 549–576.

[4] P. Lin, F. Yan, H. L. W. Chan, *Appl. Mater. Interfaces* **2010**, *2*, 1637.

[5] A. Romeo, A. Dimonte, G. Tarabella, P. D'Angelo, V. Erokhin, S. Iannotta, *APL Mater.* **2015**, *3*, 014909.

[6] R. M. Owens, G. G. Malliaras, *MRS Bull.* **2010**, *35*, 449.

[7] G. Tarabella, A. G. Balducci, N. Coppedè, S. Marasso, P. D'Angelo, S. Barbieri, M. Cocuzza, P. Colombo, F. Sonvico, R. Mosca, S. Iannotta, *Biochim. Biophys. Acta* **2013**, *1830*, 4374.

[8] H. Tang, P. Lin, H. L. W. Chan, F. Yan, *Biosens. Bioelectron.* **2011**, *26*, 4559.

[9] A. Romeo, G. Tarabella, P. D'Angelo, C. Caffarra, D. Cretella, R. Alfieri, P. G. Petronini, S. Iannotta, *Biosens. Bioelectron.* **2015**, *68*, 791.

[10] L. H. Jimison, S. A. Tria, D. Khodagholy, M. Gurfinkel, E. Lanzarini, A. Hama, G. G. Malliaras, R. M. Owens, *Adv. Mater.* **2012**, *24*, 5919.

[11] R. A. Green, N. H. Lovell, G. G. Wallace, L. A. Poole-Warren, *Biomaterials* **2008**, *29*, 3393.

[12] Y. Fang, X. Li, Y. Fang, *J. Mater. Chem. C* **2015**, *3*, 6424.

[13] D. Khodagholy, T. Doublet, P. Quilichini, M. Gurfinkel, P. Leleux, A. Ghestem, E. Ismailova, T. Hervé, S. Sanaur, C. Bernard, G. G. Malliaras, *Nat. Commun.* **2013**, *4*, 1575.

[14] P. Gkoupidenis, D. A. Koutsouras, T. Lonjaret, J. A. Fairfield, G. G. Malliaras, *Nat. Publ. Gr.* **2016**, 1.

[15] D. Balma, A. Lamberti, S. L. L. Marasso, D. Perrone, M. Quaglio, G. Canavese, S. Bianco, M. Cocuzza, *Microelectron. Eng.* **2011**, *88*, 2208.

[16] A. Tommasi, M. Cocuzza, D. Perrone, C. Pirri, R. Mosca, M. Villani, N. Delmonte, A. Zappettini, D. Calestani, S. Marasso, *Sensors* **2017**, *17*, 62.

[17] S. L. Marasso, A. Tommasi, D. Perrone, M. Cocuzza, R. Mosca, M. Villani, A. Zappettini, D. Calestani, *Nanotechnology* **2016**, *27*, 1.

[18] I. Para, S. L. Marasso, D. Perrone, M. G. Gentile, C. Sanfilippo, G. Richieri, L. Merlin, D. Pugliese, M. Cocuzza, S. Ferrero, L. Scaltrito, C. F. Pirri, *IEEE Trans. Electron Devices* **2017**, *64*, 4226.

[19] V. Dubois, S. J. Bleiker, G. Stemme, F. Niklaus, *Adv. Mater.* **2018**, *1801124*, 1801124.

[20] Y. Yoshimura, Y. Takeda, K. Fukuda, D. Kumaki, S. Tokito, *Org. Electron. physics, Mater. Appl.* **2014**, *15*, 2696.

[21] B. D. Nilsson, M. Chen, T. Kugler, T. Remonen, M. Armgarth, M. Berggren, *Adv. Mater.* **2002**, *14*, 51.

[22] K. Tybrandt, I. V. Zozoulenko, M. Berggren, *Sci. Adv.* **2017**, *3*, eaao3659.

[23] J. Bobacka, A. Lewenstam, A. Ivaska, *J. Electroanal. Chem.* **2000**, *489*, 17.

[24] A. V. Volkov, K. Wijeratne, E. Mitraka, U. Ail, D. Zhao, K. Tybrandt, J. W. Andreasen, M. Berggren, X. Crispin, I. V. Zozoulenko, *Adv. Funct. Mater.* **2017**, *27*, 1700329.

[25] K. Tsukagoshi, F. Fujimori, T. Minari, T. Miyadera, T. Hamano, Y. Aoyagi, *Appl. Phys. Lett.* **2007**, *91*, 113508(3).

[26] M. Weis, K. Lee, D. Taguchi, T. Manaka, M. Iwamoto, *Jpn. J. Appl. Phys.* **2012**, *51*, 100205.

[27] A. M. Nardes, M. Kemerink, R. A. J. J. Janssen, *Phys. Rev. B - Condens. Matter Mater. Phys.* **2007**, *76*, 085208.

[28] S. Khodakarimi, M. H. Hekhmatshoar, M. Nasiri, M. Khaleghi Moghaddam, F. Abbasi, *J. Mater. Sci. Mater. Electron.* **2016**, *27*, 1278.

[29] X. Crispin, F. L. E. Jakobsson, a Crispin, P. C. M. Grim, P. Andersson, a Volodin, C. van Haesendonck, M. Van der Auweraer, W. R. Salaneck, M. Berggren, *Chem. Mater.* **2006**, *18*, 4354.

[30] V. Preziosi, M. Barra, A. Perazzo, G. Tarabella, R. Agostino, S. L. Marasso, P. D'Angelo, S. Iannotta, A. Cassinese, S. Guido, *J. Mater. Chem. C* **2017**, *5*, 2056.

[31] J. Rivnay, P. Leleux, M. Ferro, M. Sessolo, A. Williamson, D. a. Koutsouras, D. Khodagholy, M. Ramuz, X. Strakosas, R. M. Owens, C. Benar, J.-M. Badier, C. Bernard, G. G. Malliaras, *Sci. Adv.* **2015**, *1*, e1400251.

[32] D. Khodagholy, M. Gurfinkel, E. Stavrinidou, P. Leleux, T. Herve, S. Sanaur, G. G. Malliaras, *Appl. Phys. Lett.* **2011**, *99*, 163304.

[33] P. D'Angelo, G. Tarabella, A. Romeo, S. Marasso, A. Verna, M. Cocuzza, C. Peruzzi, D. Vurro, S. Iannotta, *Materials (Basel).* **2018**, *12*, 9.

[34] M. J. Donahue, A. Williamson, X. Strakosas, J. T. Friedlein, R. R. McLeod, H. Gleskova, G. G. Malliaras, *Adv. Funct. Mater.* **2017**, *30*, 1705031.

[35] Q. Thiburce, A. Giovannitti, I. McCulloch, A. J. Campbell, *Nano Lett.* **2019**, *19*, 1712.

[36] D. Demarchi, P. Civera, G. Piccinini, M. Cocuzza, D. Perrone, *Electrochim. Acta* **2009**, *54*, 6003.

[37] I. Rattalino, P. Motto, G. Piccinini, D. Demarchi, *Phys. Lett. A* **2012**, *376*, 2134.

[38] P. Motto, M. Crepaldi, G. Piccinini, D. Demarchi, *IEEE Trans. Nanotechnol.* **2014**, *13*, 322.

[39] S. Ouyang, Y. Xie, D. Zhu, X. Xu, D. Wang, T. Tan, H. H. Fong, *Org. Electron. physics, Mater.*

Appl. **2014**, *15*, 1822.

[40] P. G. Taylor, J. K. Lee, A. A. Zakhidov, M. Chatzichristidi, H. H. Fong, J. A. DeFranco, G. G. Malliaras, C. K. Ober, *Adv. Mater.* **2009**, *21*, 2314.

[41] D. Khodagholy, J. Rivnay, M. Sessolo, M. Gurfinkel, P. Leleux, L. H. Jimison, E. Stavrinidou, T. Herve, S. Sanaur, R. M. Owens, G. G. Malliaras, *Nat. Commun.* **2013**, *4*, 2133.

[42] J. Rivnay, P. Leleux, M. Sessolo, D. Khodagholy, T. Hervé, M. Fiocchi, G. G. Malliaras, *Adv. Mater.* **2013**, *25*, 7010.

[43] U. A. Aregueta-Robles, A. J. Woolley, L. A. Poole-Warren, N. H. Lovell, R. A. Green, *Front. Neuroeng.* **2014**, *7*, DOI 10.3389/fneng.2014.00015.

[44] J. Rivnay, P. Leleux, M. Ferro, M. Sessolo, A. Williamson, D. A. Koutsouras, D. Khodagholy, M. Ramuz, X. Strakosas, R. M. Owens, C. Benar, J. Badier, C. Bernard, G. G. Malliaras, *Sci. Adv.* **2015**, 1.

[45] C. Ocampo, R. Oliver, E. Armelin, C. Alemán, F. Estrany, *J. Polym. Res.* **2006**, *13*, 193.

[46] E. Barrera Ramirez, Characterization of a PEDOT:PSS Electrolytic Device Using an in Situ Spectroelectrochemical Technique, Carleton University, Ottawa, **2013**.

[47] P. D'Angelo, N. Coppedè, G. Tarabella, A. Romeo, F. Gentile, S. Iannotta, E. Di Fabrizio, R. Mosca, *Org. Electron.* **2014**, *15*, 3016.

[48] C. M. Proctor, J. Rivnay, G. G. Malliaras, *J. Polym. Sci. Part B Polym. Phys.* **2016**, 1.

[49] B. E. Conway, *Kluwer Acad.* **1999**, *10*, 221.

[50] E. Stavrinidou, P. Leleux, H. Rajaona, D. Khodagholy, J. Rivnay, M. Lindau, S. Sanaur, G. G. Malliaras, *Adv. Mater.* **2013**, *25*, 4488.

[51] D. Bernards, G. G. Malliaras, *Adv. Funct. Mater.* **2007**, *17*, 3538.

[52] G. C. Faria, D. T. Duong, A. Salleo, *Org. Electron.* **2017**, *45*, 215.

[53] G. Tarabella, C. Santato, S. Y. Yang, S. Iannotta, G. G. Malliaras, F. Cicoira, *Appl. Phys. Lett.*

2010, *97*, 123304.

[54] T. Stöcker, A. Köhler, R. Moos, *J. Polym. Sci. Part B Polym. Phys.* **2012**, *50*, 976.

[55] M. Rudolph, E. L. Ratcliff, *Nat. Commun.* **2017**, *8*, 1048.

[56] A. M. Nardes, M. Kemerink, R. A. J. Janssen, J. A. M. Bastiaansen, N. M. M. Kiggen, B. M. W. Langeveld, A. J. J. M. Van Breemen, M. M. De Kok, *Adv. Mater.* **2007**, *19*, 1196.

[57] A. Amirudin, D. Thieny, *Prog. Org. Coatings* **1995**, *26*, 1.

[58] L. Jianguo, G. Gaoping, Y. Chuanwei, *Electrochim. Acta* **2005**, *50*, 3320.

[59] P. Civera, D. Demarchi, G. Piccinini, M. Cocuzza, D. Perrone, in *Proc. - IEEE Int. Work. Des. Test Nano Devices, Circuits Syst. NDCS 2008*, **2008**, pp. 11–14.

[60] A. Verna, S. L. Marasso, P. Rivolo, M. Parmeggiani, M. Laurenti, M. Cocuzza, *Micromachines* **2019**, *10*, 426.

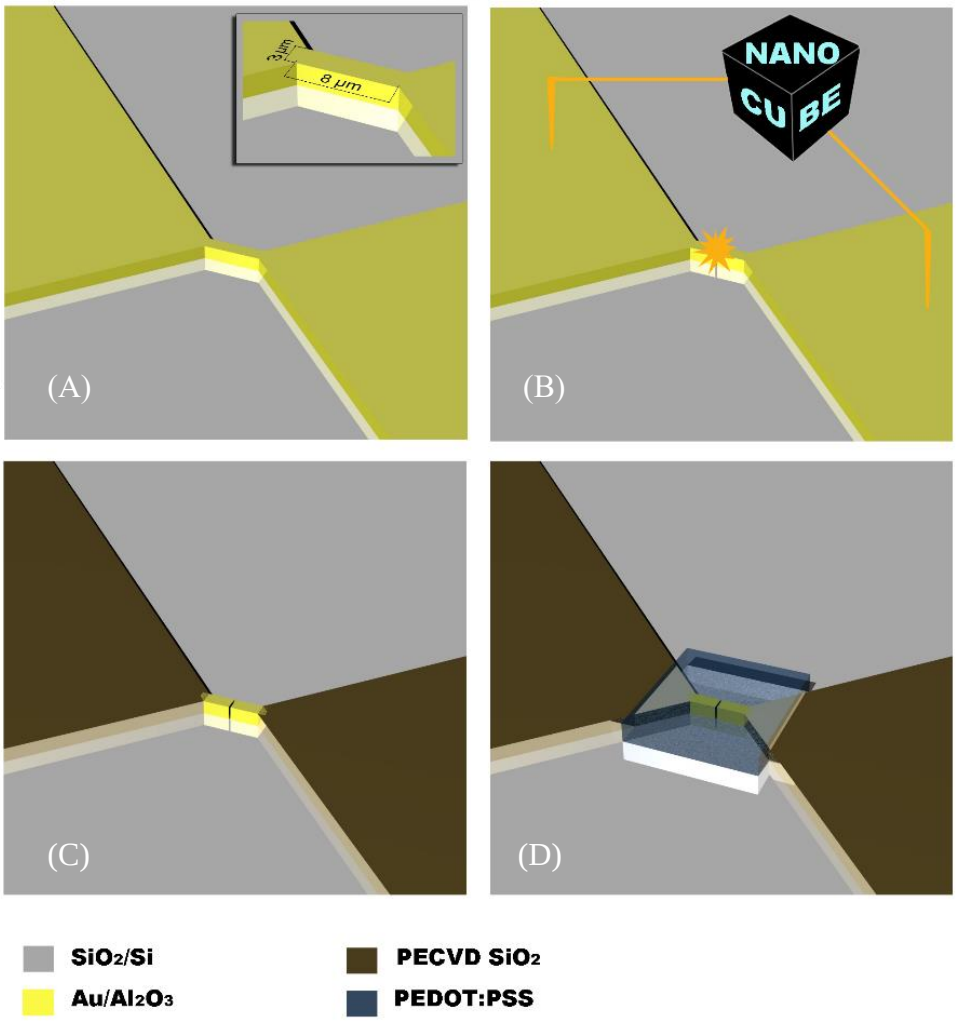
3 µm
8 µm
NANO
CU BE
(A)
(B)
(C)
(D)
SiO2/Si
Au/Al2O3
PECVD SiO2
PEDOT:PSS

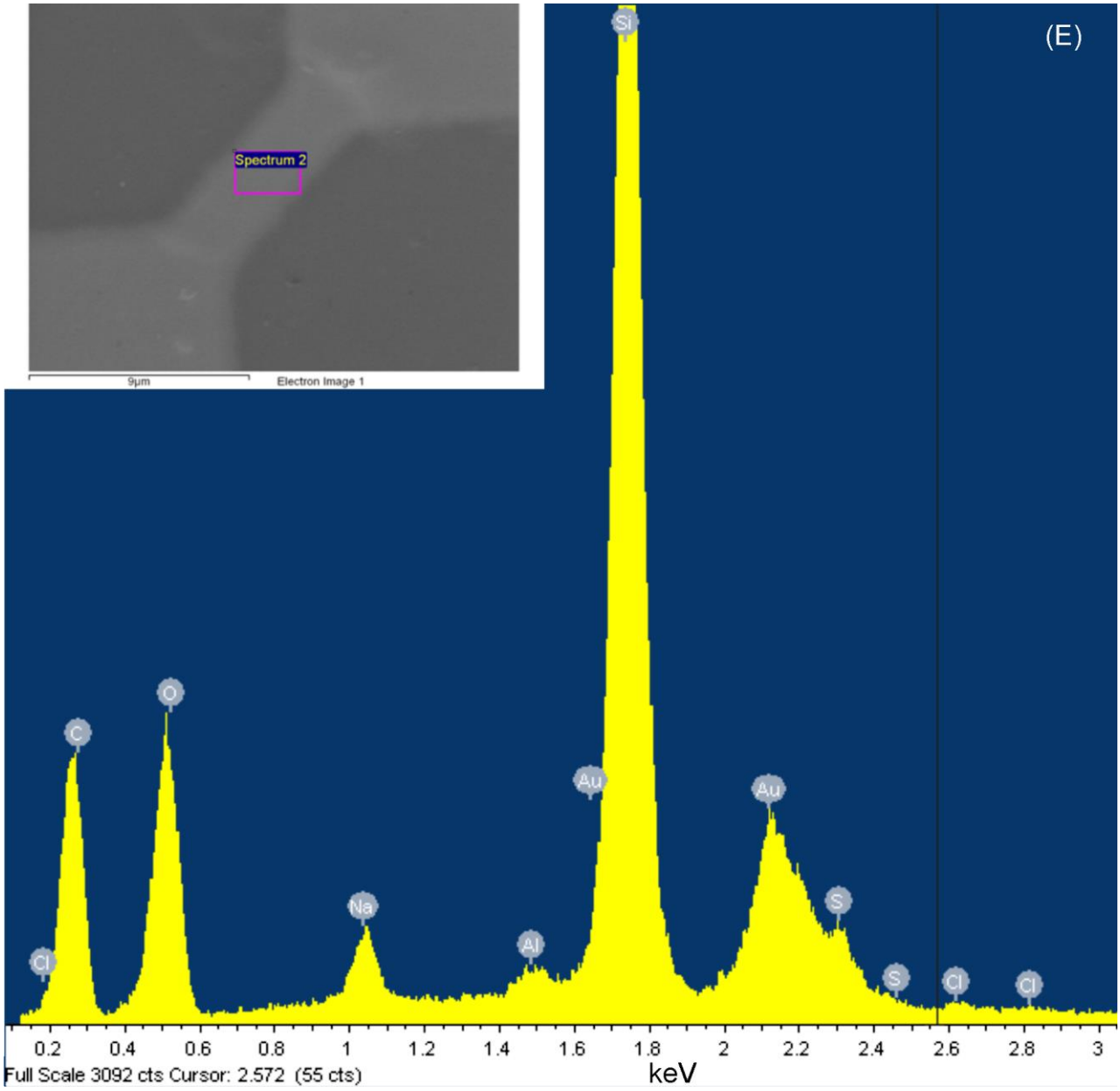

Figure 1. (A) Au microwire (8 µm in length and 2 µm in width) fabrication by Au/Al_2O_3 deposition and patterning; (B) Nanogap formation by EIBJ; (C) contacts passivation; (D) PEDOT:PSS deposition and patterning; (E) EDS spectrum of the central area of the final Nanogap-OECT characterized in NaCl electrolyte solution (in the inset the FESEM image of the investigation area).

Table 1. EDS analysis report on the Nanogap-OECT.

Element	Weight%	Atomic%	Emission peaks
C	35.18	54.63	K
O	21.55	25.12	K
Na [a)]	1.56	1.27	K
Al	0.43	0.30	K

Si	23.93	15.89	K
S	2.06	1.20	K
Cl [a)]	0.32	0.17	K
Au	14.97	1.42	M

[a)] residual contamination due to OECT characterization in NaCl solution

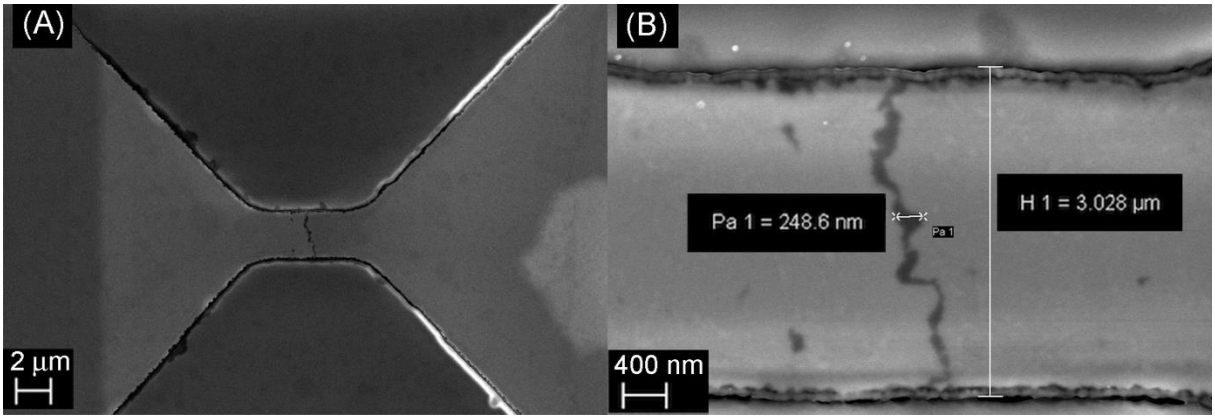

Figure 2. FESEM image of a submicrometric gap obtained by EIBJ of an Au micro wire: (A) low magnification image (10000 ×) and (B) high magnification image (65000 ×).

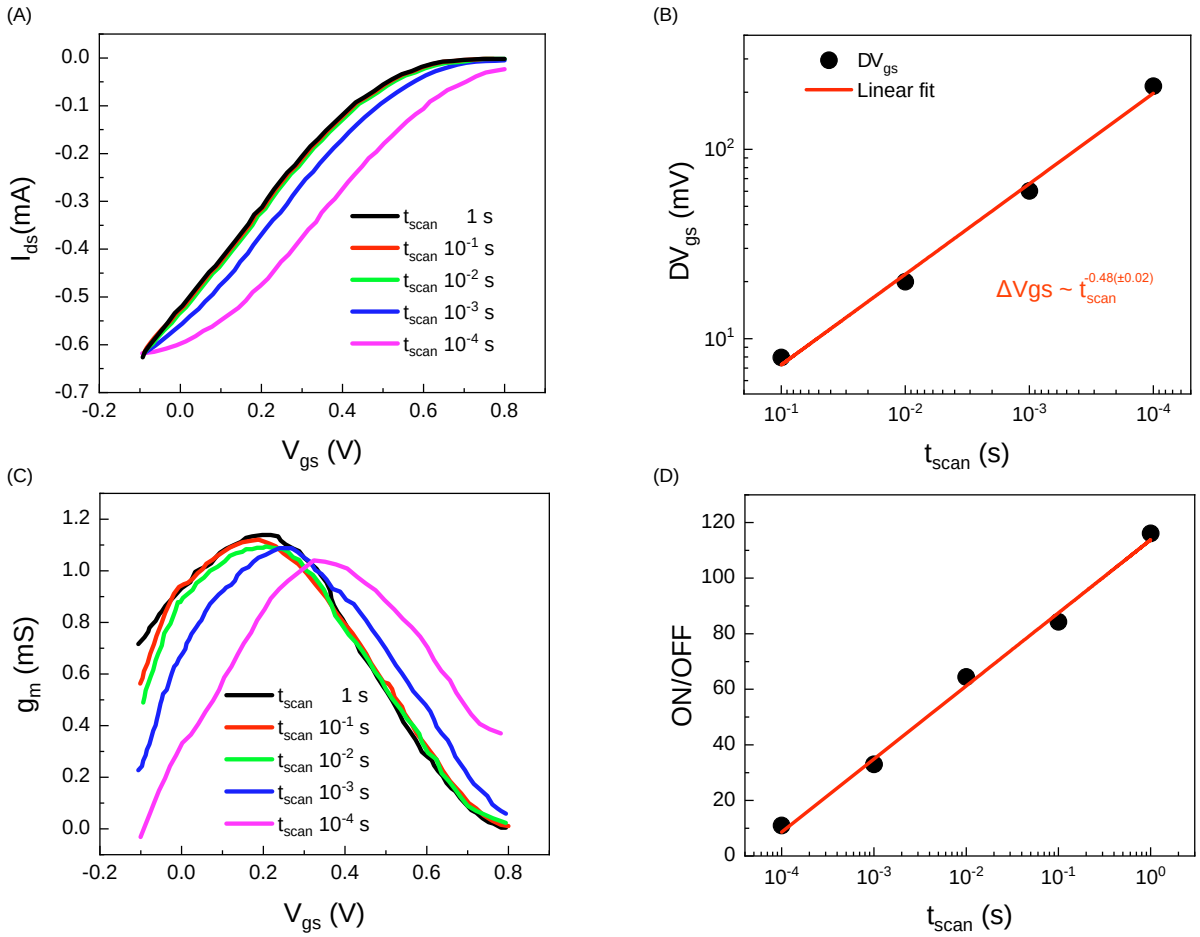

Figure 3. (A) Transfer curves I_{ds} vs. V_{gs} recorded @ V_{ds}=-0.2V by varying V_{gs} between -0.1 V and 0.8 V (V_{gs} scan step of 0.01 V), for different scan times: t_{scan}= 100 µs (magenta), 1 ms (blue), 10 ms (green), 100 ms (red) and 1 s (black); (B) log-log plot of ΔV_{gs} vs. t_{scan} and related fitting curve (red line; $\Delta V_{gs} \sim t_{scan}^{-(0.48\pm0.02)}$); (C) transconductance curves (calculated as $g_m = \partial I_{ds}/\partial V_{gs}$ from the transfer curves reported in (A)) as a function of t_{scan}; (D) ON-OFF ratio as a function of log(t_{scan})(fit curve, red line).

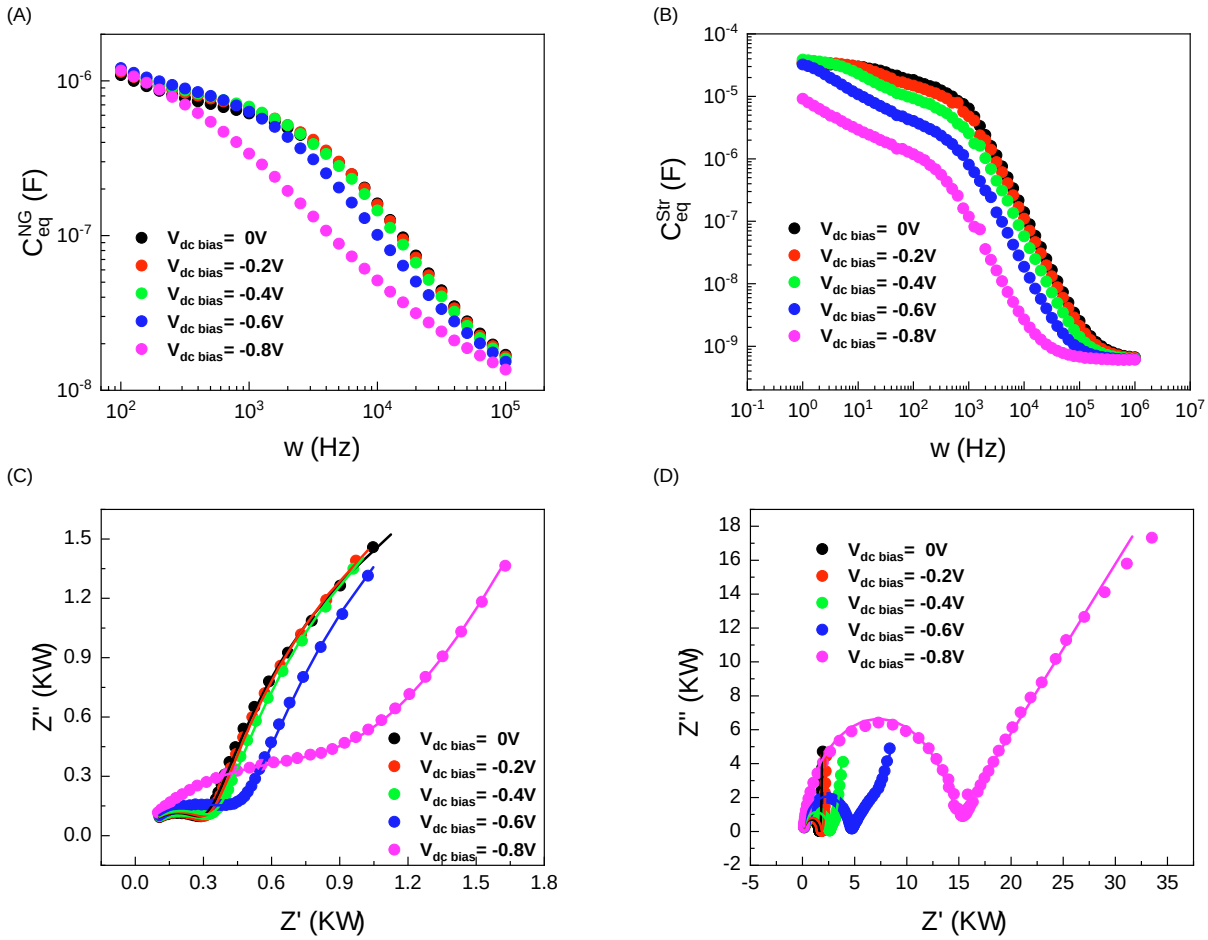

Figure 4. Equivalent capacitance C_{eq} (=1/(2πfZ'')) as a function of the ac signal frequency (± 10 mV) in the case of (A) a Nanogap-OECT and (B) a stripe-like OECT, recorded in presence of the superimposed dc biases; Nyquist plots in presence of negative dc biases for (C) a Nanogap-OECT and (D) a stripe-like OECT; fitting curves (as line plots) upon equivalent circuit analysis are reported too. For all the reported measurements, $V_{dc\ bias}$=0 (black symbols-lines), $V_{dc\ bias}$=-0.2 (red symbols-lines), $V_{dc\ bias}$=-0.4 (green symbols-lines), $V_{dc\ bias}$=-0.6 (blue symbols-lines) and $V_{dc\ bias}$=-0.8 V (magenta symbols-lines).

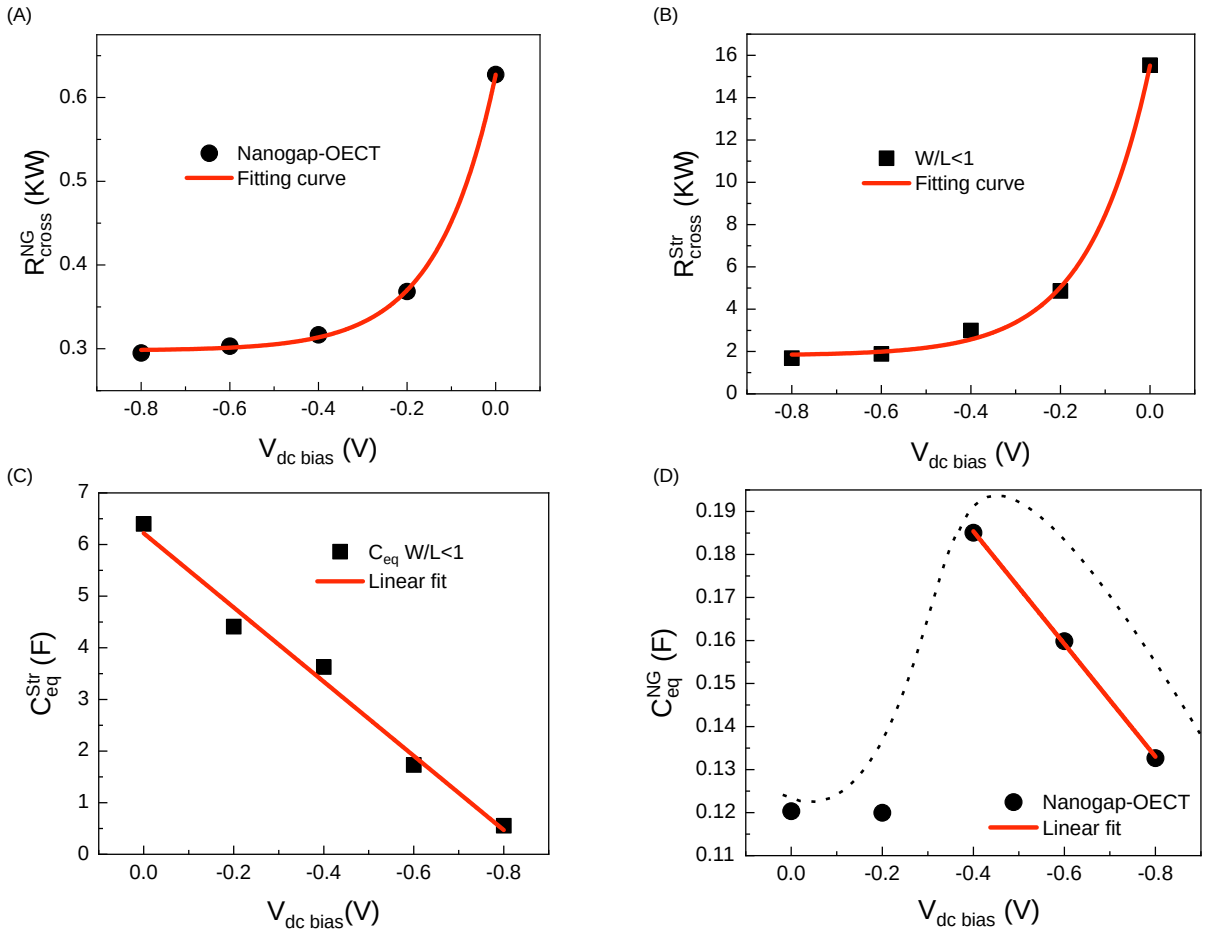

Figure 5. Resistive contribution to the total impedance at the crossover between a regime where the electrochemical response is controlled by charge transfer mechanisms and a regime showing a diffusion limited behavior in the case of (A) a Nanogap-OECT and (B) a stripe-like OECT. Ceq as a function of Vdc bias for (C) a stripe-like OECT and (D) a Nanogap-OECT. The related fitting curves (red curves and lines) are reported in all cases.

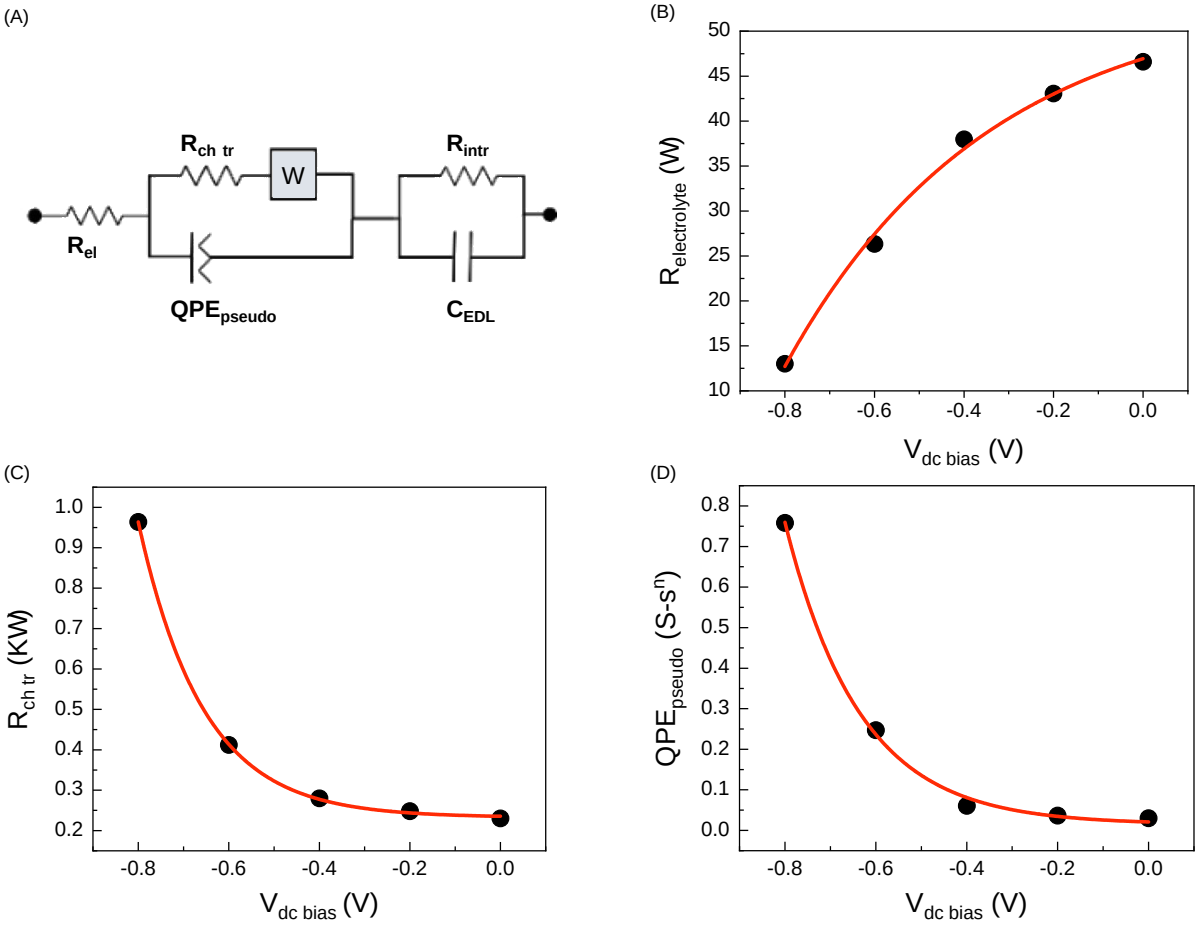
(A)
$R_{ch\ tr}$
W
R_{intr}
R_{el}
QPE_{pseudo}
C_{EDL}
(B)
$R_{electrolyte}$ (W)
$V_{dc\ bias}$ (V)
(C)
$R_{ch\ tr}$ (KW)
$V_{dc\ bias}$ (V)
(D)
QPE_{pseudo} ($S\text{-}s^n$)
$V_{dc\ bias}$ (V)

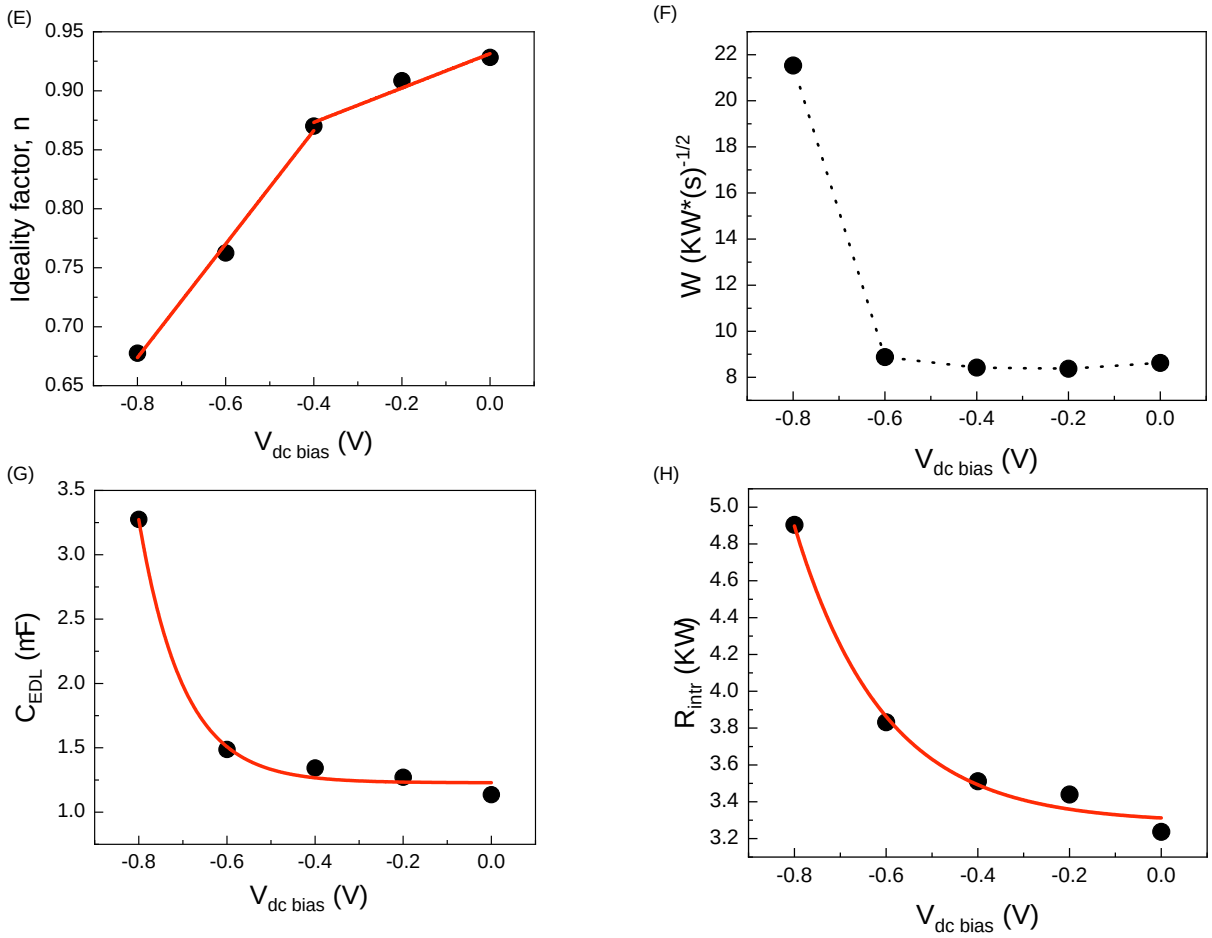

Figure 6. (A) Randles Mixed Kinetic-Charge Transfer Control equivalent circuit in series with intrinsic contribution to the impedance; (B) resistive contribution of the electrolyte resistance $R_{electrolyte}$ as a function of dc bias voltages and related fitting curve (red curve); (C) charge transfer resistance $R_{ch\text{-}tr}$ as a function of $V_{dc\ bias}$ (fitting curve in red); (D) QPE_{pseudo} and (E) ideality factor n vs. $V_{dc\ bias}$ with related exponential and linear fitting curves, respectively; (F) Warburg coefficient as a function of $V_{dc\ bias}$; (G) intrinsic electrical double layer capacitance C_{EDL} as a function of $V_{dc\ bias}$ and related exponential fitting curve (red curve);(H) resistive contribution due to intrinsic charge transport as a function of $V_{dc\ bias}$ (fitting curve in red).

Table 2. Fitting parameters for the stripe-like OECT evaluated for an equivalent circuit made of a Mixed Kinetic-Charge Transfer Control in series with a constant phase element mimicking pseudocapacitive effects.

$V_{dc\ bias}$ [V]	R_{el} [Ω]	$R_{ch\text{-}tr}$ [Ω]	QPE1 [$S*s^n$]	n	W [$Ω*s^{-1/2}$]	QPE2 [$S*s^n$]
0	114	1501	0.001	0.991	1167	35.4
-0.2	114.7	1711	0.001	0.993	1939	38
-0.4	114.1	2424	0.001	0.995	4233	53
-0.6	110	4406	0.001	0.999	11600	36
-0.8	107.4	14130	0.001	1.010	43600	[a]

[a)] For a stripe-like OECT, the Mixed Kinetic-Charge Transfer Control equivalent circuit alone well describes the Nyquist plot at Vdc bias=-0.8 V.

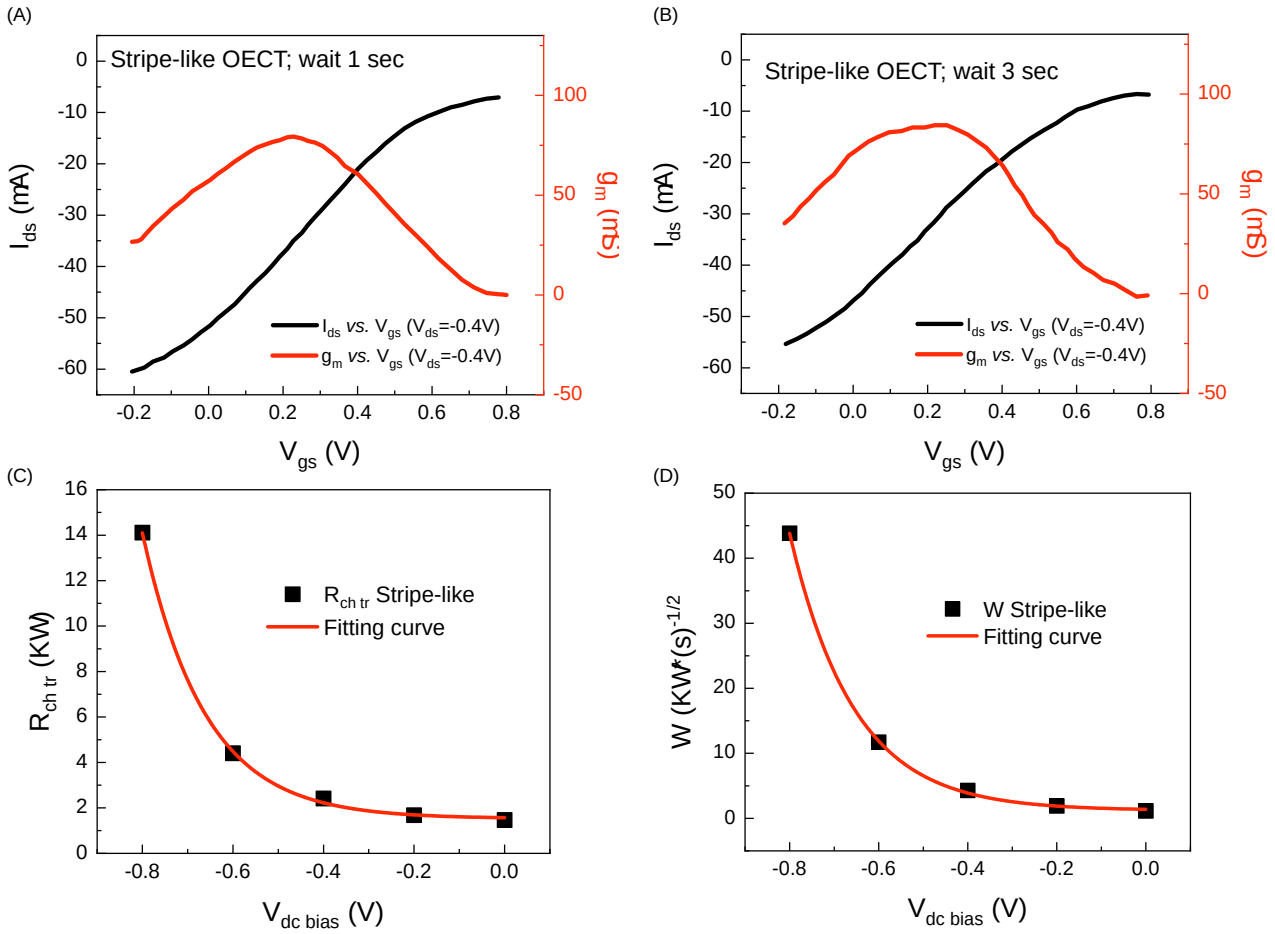

Figure 7. Transfer curves (black line) and transconductance (red line) as a function of V_{gs} for a stripe-like OECT at t_{scan} =1 s (A) and 3 s (B); (C) charge transfer resistance ($R_{ch\text{-}tr}$) and (D) Warburg coefficient (W) reported in Table 2 as a function of $V_{dc\ bias}$ (fitting curves in red) for a stripe-like OECT.

A smart approach to the fabrication of sub-micrometer channel sized Organic Electrochemical Transistors (herein referred to as Nanogap-OECTs) by an Electromigration Induced Break Junction (EIBJ) method is presented. Basic mechanism and key parameters affecting the Nanogap-OECTs characteristics (i.e. response speed and amplification) are analyzed and elucidated through Electrical and Electrochemical Impedance Spectroscopy characterization.

Keyword Nanogap-OECTs

Pasquale D'Angelo ‡, Simone L. Marasso ‡*, Alessio Verna, Alberto Ballesio, Matteo Parmeggiani, Alessandro Sanginario, Giuseppe Tarabella, Danilo Demarchi, Candido F. Pirri, Matteo Cocuzza and Salvatore Iannotta.

Scaling Organic Electrochemical Transistors Down to Nano-sized Channels